Modeling and simulation of a heat generation system for a Multi-Effect Desalination plant based on solar flat-plate collectors

Gary Ampuño[1], Lidia Roca[2], Manuel Berenguel[3], Juan D. Gil[3] and Manuel Pérez[3]

[1] Universidad Politécnica Salesiana, Guayaquil (Ecuador)

[2] CIEMAT-Plataforma Solar de Almería, Centro Mixto CIESOL, Tabernas, (Spain)

[3] Universidad de Almería, Centro Mixto CIESOL, ceiA3, Almería, (Spain)

Abstract

This paper outlines the development of models of a solar-assisted heat generation system for a Multi-Effect Desalination (MED) plant, to be used both for simulation and control purposes. Some of these models have been developed based on static and dynamic energy and mass balances, and some others are based on step response methods (experimental tests). The heat generation system comprises a solar flat-plate collector field, an air cooler, a heat exchanger and the corresponding pipelines and interconnections. The main purpose of the heat generation system is to feed the MED unit with hot water within a specific temperature range using two thermal storage tanks as input buffers to the MED system. The main achievement of this paper is that the developed model provides an adequate tradeoff between complexity and performance.

Keywords: *dynamic simulation, solar energy, solar desalination process*

1. Introduction

Fresh water scarcity and increasing concentration of greenhouse gases (mainly caused by humans) are an important problem nowadays. Solar desalination has been studied for several years to provide fresh water and minimize CO_2 footprint. The use of solar energy for desalination processes can be done using multi-effect distillation (MED) coupled to a thermal solar energy system, which is known as indirect solar distillation.

During the last years, different solar-powered desalination technologies have been tested at Plataforma Solar de Almeria (PSA), a dependency of the CIEMAT (Centro de Investigaciones Energéticas, Medioambientales y Tecnológicas), a public research body assigned to the Spanish Ministry of Economy, Industry and Competitiveness. One of the research lines of the Solar Desalination Unit at PSA (South East Spain) is the integration of solar facilities into desalination processes, requiring validated dynamic models to design and test control strategies to improve the operating process. The solar field lumped parameter model presented in Camacho et al. (2012) has been widely used for control purposes not only for parabolic trough collectors (Cirre et al., 2007; Romera Cabrerizo and Santos, 2017), but also for compound parabolic collectors (Roca et al., 2008; Ayala et al., 2011, Torrico et al., 2009 and 2010) and flat-plate solar fields (Gil et al., 2015). This kind of simple but accurate models can be used also for optimization studies to maximize economic benefits (González et al., 2014) or to reduce costs (Roca et al., 2016). For the case of the Multi-Effect Desalination (MED) unit, a detailed model based on energy and mass balances was developed and validated with real data (de la Calle et al., 2015) and used to determine the optimal operating points taking into account different performance indexes (Carballo et al., 2016). In all of these cases, a fundamental issue is to develop models that account for a performance/accuracy tradeoff to obtain reliable results in a low computational time.

This paper shows the modeling and simulation of the heat generation system used in the AQUASOL-II solar distillation plant placed at PSA. The model was developed to help analyzing different scenarios in simulation and in order to design, develop and test control algorithms aimed at improving the operation of this kind of plants. This model includes:

- the solar field, to gather the thermal solar energy,
- an air cooler, able to reduce the temperature at the end of the solar field, and,
- a heat exchanger (HX), in charge of transferring thermal energy to the water contained in the storage tanks.

The paper is organized as follows: first, AQUASOL-II plant is explained in section 2, followed by the implementation of models in section 3. A comparison between experimental and simulation results is performed in section 4 and some concluding remarks are finally drawn.

2. The solar plant and MED unit

The solar desalination facility AQUASOL-II (see Fig. 1) has a flat-plate solar field to supply process heat to an industrial system, in this case, the MED system. This plant was designed and built with the aim of studying the efficiency of large-aperture static solar collectors when they are coupled to desalination processes. Fig. 1 also shows the layout of this facility which basically consists of two main circuits; the primary circuit is the heat generation system and the secondary circuit is the consumer system composed by two water storage tanks and the MED unit.

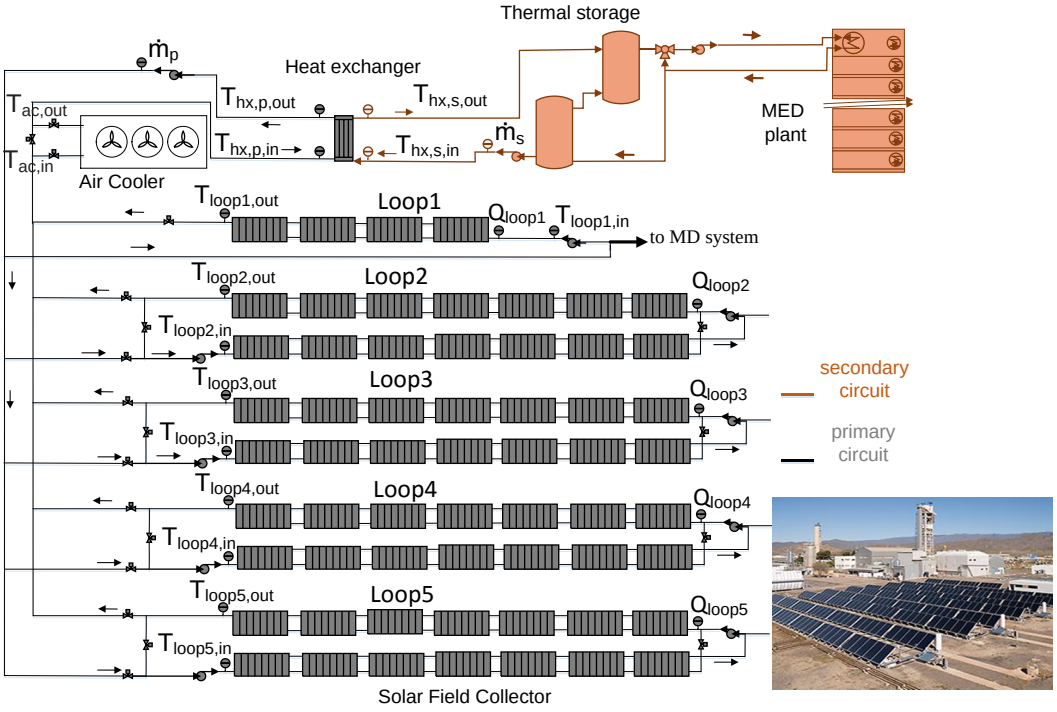

Fig. 1: Schematic diagram of the solar MED facility at PSA and photo of the solar field.

This work deals with the modeling and simulation of the primary circuit, the solar-based heat generation system, comprising the solar field, an air cooler, a heat exchanger and connection pipes. The static solar field (Distributed Collector System, DCS) is composed of 60 collectors (LBM HTF by WAGNER & Co) distributed in five loops connected in parallel. There are four loops with 14 flat-plate collectors each (each loop has two rows connected in series with 7 collectors in parallel per row) and one loop with 4 flat-plate collectors connected in parallel. Each loop has its own pumping system so that it can be operated independently. For example, loop 1 can be used to feed a solar membrane distillation (MD) system with thermal energy. As the main energy source, the solar irradiance, cannot be manipulated (it acts as a disturbance from the control viewpoint), the outlet temperature of the solar field is usually controlled by manipulating the flow using the pumps (Roca et al., 2009). Depending on the operating requirements (solar field characterization, or process heat for the desalination unit) the hot fluid from the solar field enters an air cooler or directly reaches a heat exchanger to heat the secondary water circuit where thermal storage tanks are placed. Table 1 describes the nomenclature used in this work.

Table.1: Nomenclature

Symbol	Description	Unit
A	Cross-sectional area of the loop pipe	m^2
A_{cs}	Collector absorber cross-sectional area	m^2
A_{hx}	heat exchange surface	m^2
c_p	Specific heat capacity	$J \cdot kg^{-1} \cdot {}^oC^{-1}$
c_f	Conversion factor to account for number of modules, connections and L/min conversion	$s \cdot L \cdot min^{-1} \cdot m^{-3}$
d_{ac}	Time delay associated to air cooler	s
$d_{j,tout-I}$	Irradiance-outlet water temperature related transport delay in loop j ($j = 1..5$)	s
$d_{j,tout-Q}$	Flow rate-outlet water temperature related transport delay in loop j ($j = 1..5$)	s
$d_{j,tout-tin}$	Inlet water temperature-outlet water temperature related transport delay in loop j ($j = 1..5$)	s
H	Thermal losses coefficient	$J \cdot s^{-1} \cdot {}^oC^{-1}$
I	Solar irradiance	$W \cdot m^{-2}$
L	Loop pipe length	m
L_{eq}	Equivalent length of the flat plate collector tube	m
$\dot{m}_p$	Primary circuit mass flow rate	$kg \cdot s^1$
$\dot{m}_s$	Secondary circuit mass flow rate	$kg \cdot s^1$
Q_{loopj}	Volumetric flow rate in loop j ($j = 1..5$)	$L \cdot min^{-1}$
Q_p	Volumetric flow rate in primary circuit	$L \cdot min^{-1}$
Q_s	Volumetric flow rate in secondary circuit	$L \cdot min^{-1}$
Speed	Air cooler fan velocity	%
T_a	Ambient temperature	^oC
$T_{ac,in}$	Air cooler inlet temperature	^oC
$T_{ac,out}$	Air cooler outlet temperature	^oC
$T_{hx,p,out}$	Outlet temperature of heat exchanger primary circuit	^oC
$T_{hx,s,out}$	Outlet temperature of heat exchanger secondary circuit	^oC
$T_{hx,p,in}$	Inlet temperature of heat exchanger primary circuit	^oC
$T_{hx,s,in}$	Inlet temperature of heat exchanger secondary circuit	^oC
$T_{loopj,in}$	Inlet temperature of loop j ($j = 1..5$)	^oC
$T_{loopj,out}$	Outlet temperature of loop j ($j = 1..5$)	^oC
t_s	Sampling time	s
$\bar{T}$	Equivalent flat plate collector tube mean temperature	^oC
v	Velocity rate	$m \cdot s^{-1}$
α_{hx}	Heat transfer coefficient	$W \cdot m^{-2} \cdot {}^oC^{-1}$
β	Model parameter that modulates the solar irradiance component	m
$\eta_{hx,p}$	Compensator dimensionless factor for heat exchanger primary circuit	-
$\eta_{hx,s}$	Compensator dimensionless factor	-
ρ	Water density	$kg \cdot m^{-3}$

3. Solar assisted heat generation system model

To simulate the heat generation system, three main models must be developed: solar field, air-cooler and heat exchanger. Fig. 2 shows a scheme of the connections between these models. As it will be explained along the following sections, modelling the time delays is essential to get results close to those obtained at the real plant.

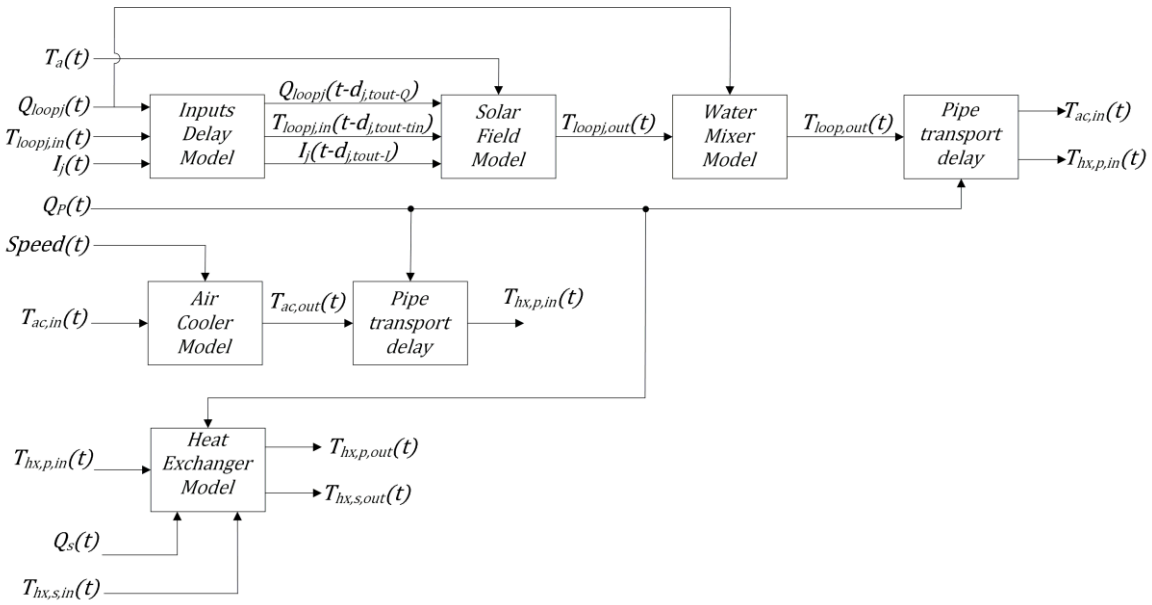

Fig. 2: Block diagram of the system model.

As will be explained in section 3.1, since the solar field model is a concentrated parameter model, some of the inputs must be delayed to reproduce the dynamic behavior of the real plant. The model provides the outlet temperature of each loop, but to calculate the temperature at the outlet of the whole solar field, pipe transport delays and energy and mass balances must be applied. These calculations are included in the block called *Water Mixer Model* in Fig. 2. Depending of the operation mode, the desired outlet can be $T_{ac,in}$ or $T_{hx,in}$ which are the inputs of the air cooler and heat exchanger model, respectively. These variables are a delayed version of $T_{loop,out}$ due to the pipe connection between devices.

It is important to mention that in the primary circuit, the temperature sensors that can be used for validation purposes are located at the end of each solar field loop and at the inlet and outlet of the heat exchanger (see Fig. 1). Therefore, to validate the solar field and air cooler models, a pipe transport delay is also applied to compare the results with the temperature located at the inlet of the heat exchanger.

3.1 Solar field model

In order to model each solar field loop, the equations presented in (Roca et al., 2009; Gil et al., 2015) have been used as reference. It is a concentrated parameter model (see Eq. 1) which provides the evolution of the outlet temperature, $T_{loopj,out}(t)$ (for the case of loop number j (j = 1..5)), considering that a hypothetical equivalent flat plate collector tube has the same behavior as the whole solar field loop. As it can be seen, the outlet temperature of the loop depends on several inputs, the manipulated one, $Q_{loopj}(t)$ is the volumetric flow, and the other ones act as disturbances: $T_{loopj,in}(t)$ is the inlet temperature, $T_a(t)$ the ambient temperature, and $I(t)$ is the solar irradiance. The equations modeling the dynamics of the outlet temperature of the loops are:

$$\rho c_p A_{cs} \frac{\partial T_{loopj,out}(t)}{\partial t} = \beta I\left(t - d_{j,tout-I}\right) - \frac{H}{L_{eq}}\left(\tilde{T}(t) - T_a(t)\right) - c_p \frac{\rho}{c_f} Q_{loopj}\left(t - d_{j,tout-Q}\right) \frac{\left(T_{loopj,out}(t) - T_{loopj,in}\left(t - d_{j,tout-tin}\right)\right)}{L_{eq}}, \quad \text{(Eq. 1)}$$

$$\tilde{T}(t) = \frac{T_{loopj,out}(t) + T_{loopj,in}(t - d_{j,tout-tin})}{2}, \quad \text{(Eq. 2)}$$

where ρ is the water density, c_p is the specific heat capacity, A_{cs} is the flat plate collector tube's cross area, L_{eq} is the length of the equivalent flat plate collector tube, H is the thermal losses coefficient $J{\cdot}s^{-1}{\cdot}{}^{o}C^{-1}$, β is a parameter that modulates the solar radiation component, $\tilde{T}(t)$ is the mean temperature of the equivalent flat

plate collector tube and c_f is a conversion factor to account for number of modules, connections and $L \cdot min^{-1}$ conversion (Gil et al., 2015). Loops from 2 to 5 have 7 collectors in each of the two rows, while loop 1 has one row of 4 collectors. Each collector has 5 panels and there are 10 absorber tubes inside each panel. The parameters are shown in Table 2.

Table. 2: Solar field variables and parameters.

Parameter	Value	Unit
c_f (conversion factor in: loop 1; loops 2..5)	$5 \cdot 4 \cdot 6 \cdot 10^5$; $5 \cdot 7 \cdot 6 \cdot 10^5$	$s \cdot L \cdot min^{-1} \cdot m^{-3}$
ρ (water density at 65 ºC)	975	$kg \cdot m^{-3}$
c_p (specific thermal capacity al 65 ºC)	$4.19 \cdot 10^3$	$J \cdot kg^{-1} \cdot ºC^{-1}$
A_{cs} (flat plate collector tube cross-section area)	$7.85 \cdot 10^{-5}$	m^2
β (irradiance model parameter)	0.0975	m
H (thermal losses coefficient for loop 1; loops 2..5)	1.1; 2.2	$J \cdot s^{-1} \cdot ºC^{-1}$
L_{eq} (equivalent flat plate collector tube length for loop 1; loops 2..5)	1.94; 3.88	m

Three different time delays have been considered in this model: $d_{j,tout\text{-}Q}$ is the delay between the outlet temperature and the inlet flow rate, $d_{j,tout-tin}$ is the delay between the outlet temperature and the inlet temperature and $d_{j,tout-I}$ is the delay between the outlet temperature and the solar irradiance. The two main reasons that cause these dead times are the transport delay in the connection pipes and the apparent delay (Normey, 2007) produced because each collector tube (which has the same behavior as a first order system with delay) is connected in parallel to the main pipe loop (see Fig.3).
From the experiments performed in this solar field, parametric equations which depend on the water flow rate have been obtained to calculate these delays:

$$d_{j,tout-Q} = 0.3 \cdot {Q_j}^2 - 23.17 \cdot Q_j + 512.97\,, \quad \text{(Eq. 3)}$$

$$d_{j,tout-tin} = 0.52 \cdot {Q_j}^2 - 40.21 \cdot Q_j + 1054, \quad \text{(Eq. 4)}$$

$$d_{j,tout-I} = 0.29 \cdot {Q_j}^2 - 22.17 \cdot Q_j + 463.58, \quad \text{(Eq. 5)}$$

$$d_{1,tout-Q} = 0.11 \cdot {Q_1}^2 - 4.33 \cdot Q_1 + 67.62, \quad \text{(Eq. 6)}$$

$$d_{1,tout-tin} = 2.6 \cdot {Q_1}^2 - 86.3 \cdot Q_1 + 876.2, \quad \text{(Eq. 7)}$$

$$d_{1,tout-I} = 0.067 \cdot {Q_1}^2 - 3.12 \cdot Q_1 + 61.1, \quad \text{(Eq. 8)}$$

where j [1,4] is the loop number.

Following the model described by Eq.1 and Eq. 2 and the delays correlations (see Eqs. 3-8), it is possible to obtain the water temperature at the outlet of each loop ($T_{loop1,out}, \ldots, T_{loop5,out}$), but to calculate the temperature at the outlet of the whole solar field ($T_{loop,out}$ in Fig.4), a steady state heat and mass balance can be applied.
Nevertheless, before this step, in order to reproduce the dynamic behavior of the temperature, it is fundamental to include the transport delays for each water element that flows between the outlet of each loop and the point of the pipe considered as $T_{loop,out}$.

In general, the transport delay between points a and b, $d_{a\text{-}b}$, can be estimated at each sampling time as a flow dependent delay as described in (Normey-Rico et al. 1998).

$$T_a(t) \approx T_b(t - d_{a-b}) \quad \text{(Eq. 9)}$$

$$L = \int_0^{d_{a-b}} v(t)\, dt \rightarrow \frac{t_s}{A} \sum_{i=0}^{i=n-1} f(k-i) = L \quad \text{(Eq. 10)}$$

where t_s is the sampling time, $v(t)$ is the velocity rate, index n is equal to the delay (in sampling times), $f(k)$ is the flow rate at sampling time k, A is the cross-section area of the loop pipe; and the integral of $v(t)$ is approximated by a discrete time sum that accounts for different flow rates.

As can be observed in Fig.4, there are different lengths and sections, and the velocity rate is also different in each section of the pipe, so the delays evaluations must be combined with the heat and mass balances. Fig. 4 shows a block diagram to follow the evaluations considered, where points P1…P4 refers to joints between loop pipes and the main pipe (see Fig. 5). Temperature mixture is evaluated inside each *E&MB* (Energy and Mass Block) component, where the implementation inside each one is the following one:

$$T_{out}(t)Q_{out}(t)c_p = \sum_{j=1}^{2} T_{in,j}(t)Q_j(t)c_p \qquad \text{(Eq. 11)}$$

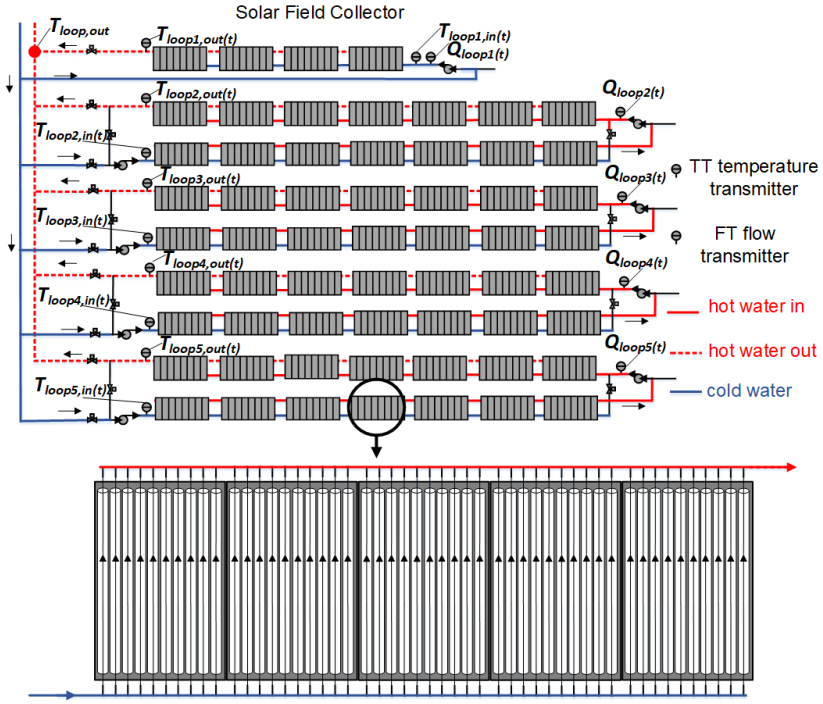

Fig. 3: Layout of AQUASOL-II solar field and detail of the tubes arrangement inside one collector module.

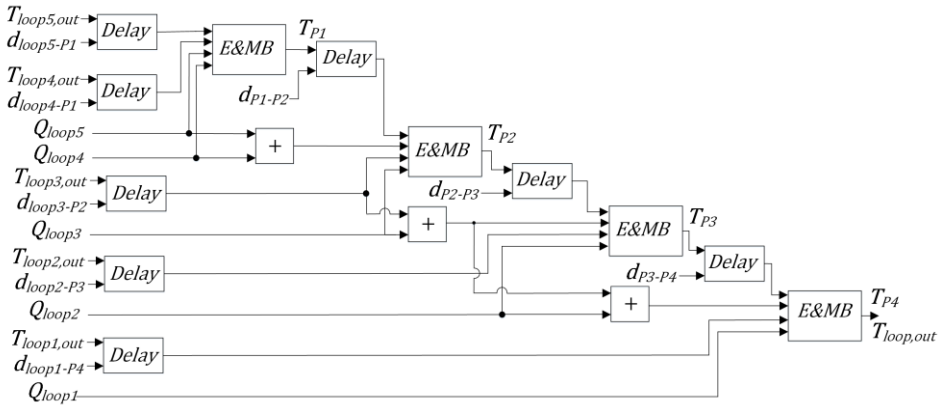

Fig. 4. Water mixture model.

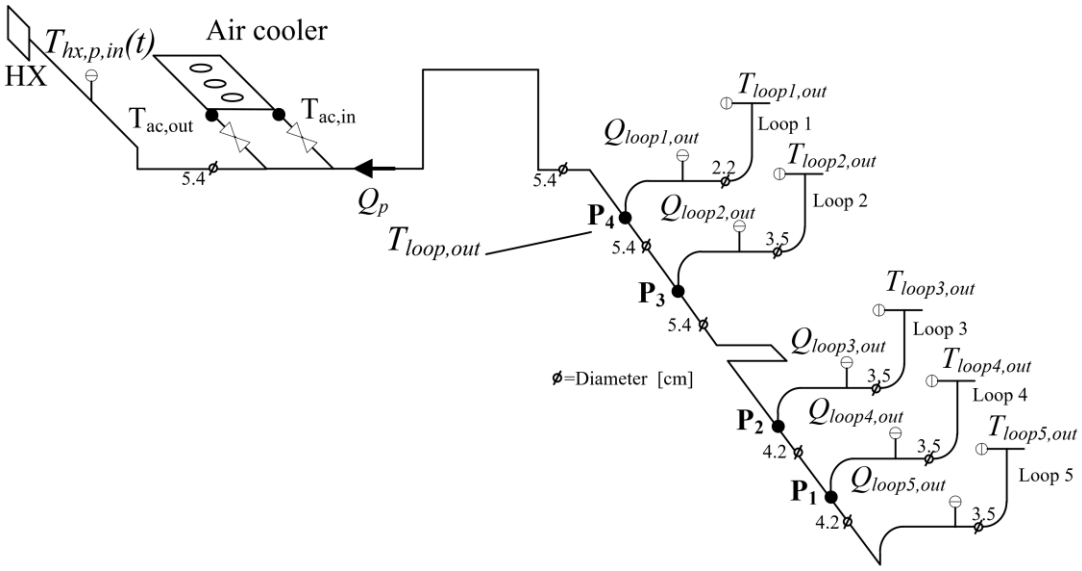

Fig. 5. Pipe sections and connections between the solar field loops and the air cooler and heat exchanger (HX).

3.2 Heat exchanger model

For the heat exchanger (HX), a static model has been implemented following the ideas of (de la Calle et al., 2015):

$$T_{hx,p,out}(t) = T_{hx,p,in}(t) - \eta_{hx,p}(t)\big(T_{hx,p,in}(t) - T_{hx,s,in}(t)\big), \quad \text{(Eq. 12)}$$

$$T_{hx,s,out}(t) = T_{hx,s,in}(t) + \eta_{hx,s}(t)\Big(T_{hx,p,in}(t) - T_{hx,p,out}(t)\Big), \quad \text{(Eq. 13)}$$

where $T_{hx,p,out}(t)$ and $T_{hx,s,out}(t)$ are the outlet temperatures and $T_{hx,p,in}(t)$ and $T_{hx,s,in}(t)$ the inlet temperatures of primary and secondary circuits respectively. In these equations, $\eta_{hx,p}(t)$ and $\eta_{hx,s}(t)$ are dimensionless factors which depends on the mass flow rates $\dot{m}_p(t)$ and $\dot{m}_s(t)$ (see Eq. 14), c_p is the specific heat, A_{hx} is the heat exchange surface and α_{hx} is the heat transfer coefficient (Table 3 includes the values of these parameters). A first order filter with representative time constant 5 has been added to this static model to better represent the evolution of the outlet temperatures.

$$\eta_{hx,p}(t) = \frac{1 - e^{\theta_{hx}}}{1 - \frac{\dot{m}_p\, c_{p,p}}{\dot{m}_s\, c_{p,s}} e^{\theta_{hx}}}; \quad \eta_{hx,s}(t) = \frac{\dot{m}_p\, c_{p,p}}{\dot{m}_s\, c_{p,s}}; \quad \theta_{hx} = \alpha_{hx} A_{hx} \left(\frac{1}{\dot{m}_p\, c_{p,p}} - \frac{1}{\dot{m}_s\, c_{p,s}}\right); \quad \text{(Eq. 14)}$$

Table 3: Heat exchanger model parameters.

Parameter	Value	Unit
Water density, ρ	975	kg m^{-3}
Specific thermal capacity, c_p	$4.19 \cdot 10^3$	J·kg^{-1}·ºC^{-1}
Heat exchange surface, A_{hx}	-	m^2
Heat transfer coefficient, α_{hx}	-	W·m^{-2}· ºC^{-1}
$\alpha_{hx}\, A_{hx}$	28000*	W· ºC^{-1}

*It was not possible get the exact independent values for α_{hx} and A_{hx} separately. A calibration procedure was performed using the model given by Eq. 11, 12 and 13, resulting a value $\alpha_{hx}\, A_{hx}$ equal to 28000 W·ºC^{-1}.

3.3 Air cooler model

To model the air cooler (AC) dynamics, a linear model has been obtained experimentally from the reaction curve method, where the input signal is the AC speed and the output is the difference between the outlet and the inlet water temperatures $\left(T_{ac,out}(t) - T_{ac,in}(t)\right)$. The corresponding transfer function in Laplace transform s is given by:

$$G(s) = -\frac{0.41}{23s + 1} \qquad \text{(Eq. 15)}$$

4. Comparison between experimental data and simulation results

This section shows the results of the models previously described and they are compared with real data from the facility. To carry on this comparison, two different kinds of experiments have been performed. To study solar efficiency, it is basic to maintain the water flow $Q_p(t)$ and solar field inlet temperature $T_{loop,in}(t)$ constant using the air cooler. In the other working mode, to heat the storage tanks, the air cooler is by-passed with manual valves and the fluid from the solar field enters directly to the heat exchanger primary circuit $T_{hx,p,in}(t)$ to heat the fluid that flows to the storage tanks. To perform the simulations the models presented previously have been connected (solar field with air cooler and solar field with heat exchanger) as presented in Fig. 2.

4.1 Solar field with air cooler

To test the solar field model validity, outlet temperature estimations are compared to data from AQUASOL-II facility (see Fig. 6) in an operating day devoted to test the efficiency of the solar field. Four loops of the solar field are working (loops 1, 3, 4 and 5), water flow rates are constant for loops 1 (11 L/min), 3 and 4 (36 L/min) whereas in loop 5 it changes from 36 L/min to 27 L/min at 10 GMT. Air cooler speed varies between 30% and 40% to maintain the inlet temperature at 60 ºC.

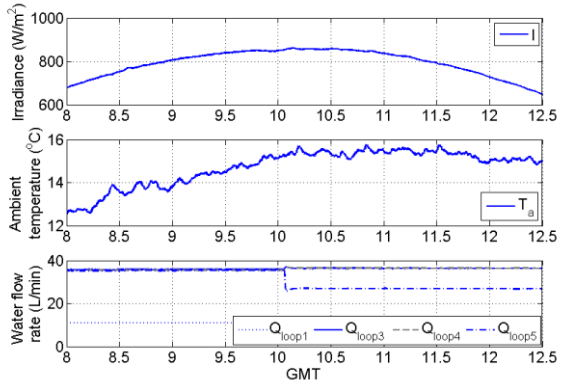

(a)

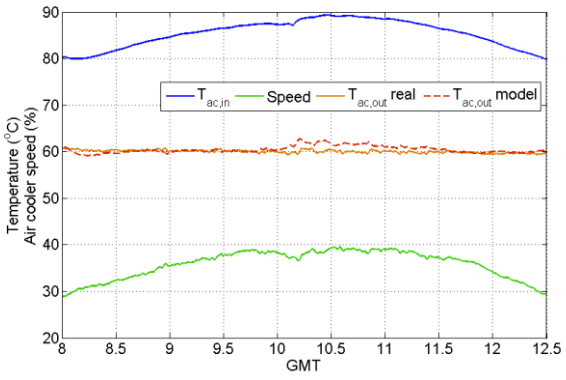

(b)

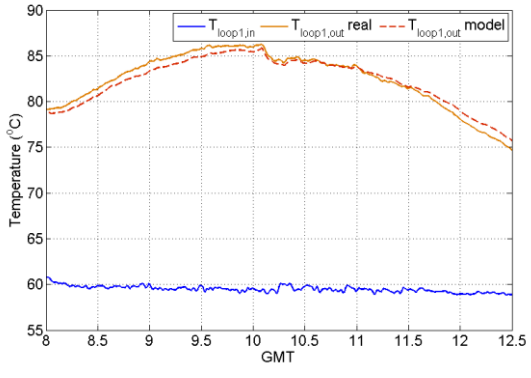

(c)

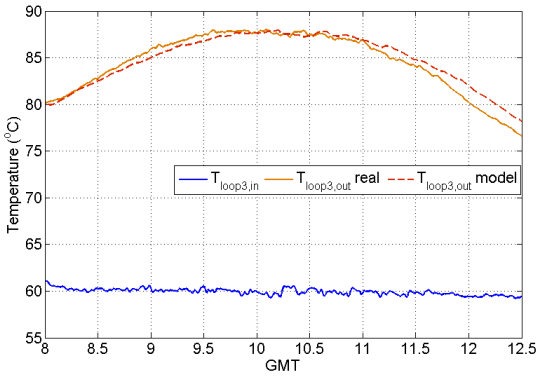

(d)

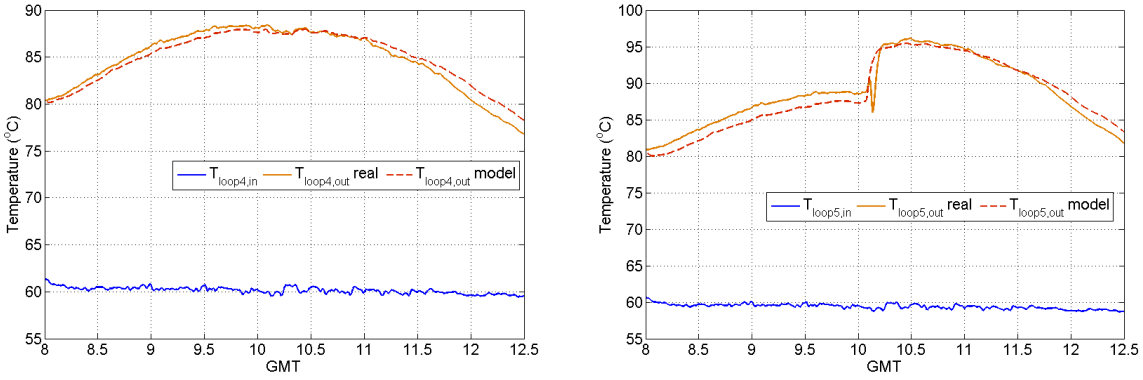

(e) (f)

Fig. 6: Solar field with air cooler model results, December 21st, 2015. (a) Solar field inputs, (b) air-cooler model results and inputs, (c) solar field loop 1 model results and inlet temperature, (d) solar field loop 3 model results and inlet temperature, (e) solar field loop 4 model results and inlet temperature, (f) solar field loop 5 model results and inlet temperature.

As can be observed, solar irradiance follows the daily cycle solar without disturbances (see Fig 6.a) and the results of the solar field model are quite good (the maximum absolute error (MAE) is 1.1 ºC, 2.6 ºC, 1.6 ºC and 6.2 ºC for loops 1, 3, 4 and 5, respectively and the root mean square error (RMSE) is 0.6 ºC, 1.3 ºC, 0.7 ºC and 1.3 ºC for loops 1, 3, 4 and 5, respectively). Notice that the huge error obtained in loop 5 occurs when the flow rate increases suddenly. This severe change may cause a hydraulic imbalance and the temperature sensor could be not completely submerged in the fluid. In the case of the air cooler model, although the RMSE is low (0.9 ºC), when the water flow rate in loop 5 changes, the outlet temperature from the model should decrease to follow the real curve. This result suggests that the model should include a dependency with the residence time of the water inside the air cooler pipe. Notice also that the air cooler model uses as inlet temperature the result from the solar field model, so that the error obtained in the solar field affects to the air cooler model error.

4.3 Solar field with heat exchanger

Fig. 7 shows representative results of the evolution of the output temperatures of the solar field and the heat exchanger. In this experiment the day presents hard disturbances in the solar irradiance, inlet flow rates are constant in the two operative loops (Q_{loop1}=14 L/min and Q_{loop4}=38 L/min) and it varies between 26 L·min^{-1} and 147 L·min^{-1} in the secondary circuit. As can be observed in Figs. 7 (b) and (c), the model follows quite well the dynamic of the real facility despite the cloud transitions, being the MAE 2.1 ºC and 3.2 ºC for loops 1 and 4, respectively, and the RMSE is 1.3 ºC and 1.8 ºC for loops 1 and 4, respectively. Fig. 7 (d) shows the heat exchanger outlet temperatures when both models are connected. As a consequence of the error committed in the solar field temperature prediction, the RMSE is 1.9 ºC and 0.5 ºC for the secondary and primary circuit, respectively, and the MAE is 5.9 ºC and 1.5 ºC for the secondary and primary circuit, respectively. If the heat exchanger model uses the measured signal $T_{hx,p,in}$ instead of the predicted one, the error is notably reduced as can be observed in Fig. 7 (e).

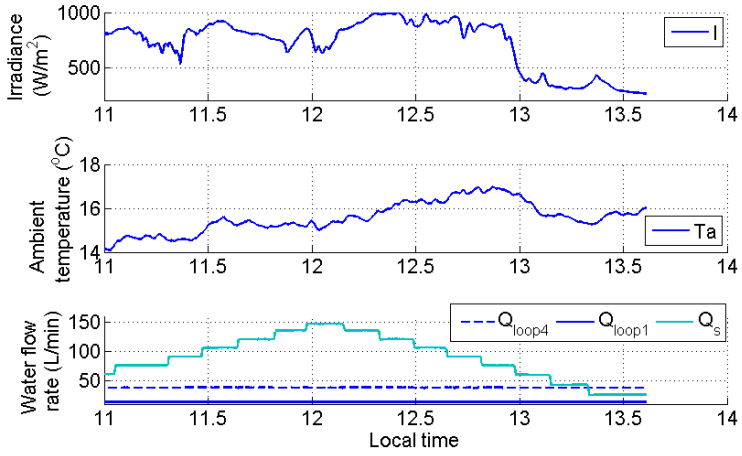

(a)

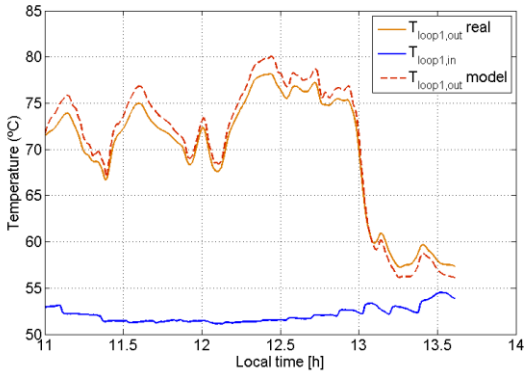

(b)

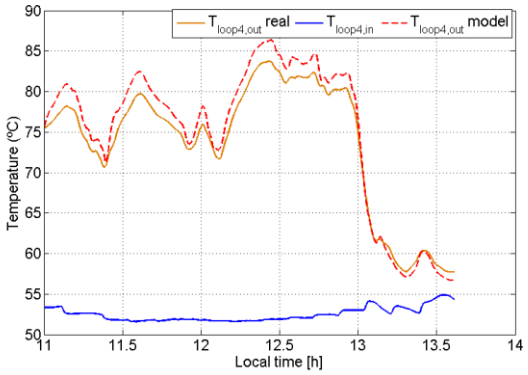

(c)

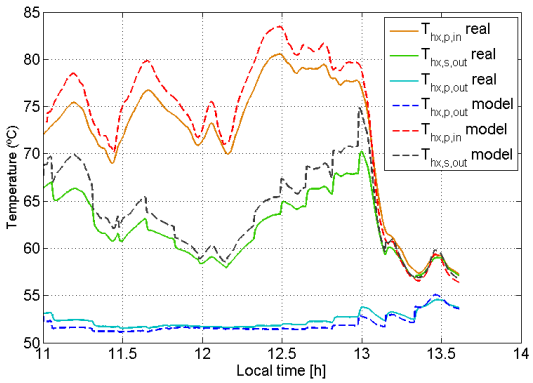

(d)

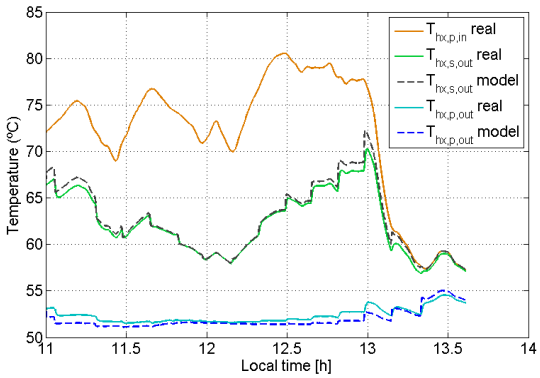

(e)

Fig. 7: Solar field with air heat exchanger model results, March 19th, 2016. (a) Model inputs (solar irradiance, ambient temperature and water flow rates), (b) solar field loop 1 model results and inlet temperature, (c) solar field loop 4 model results and inlet temperature, (d) heat exchanger model results using $T_{hx,p,in}$ from the model and (e) heat exchanger model results using the real value $T_{hx,p,in}$ from the facility.

Conclusions

This work shows the feasibility of using the developed models to simulate the outlet temperature of the AQUASOL-II facility taking into account the dynamics of the solar field, the air heater, the heat exchanger and the involved delays. The model is useful for analyzing different operating scenarios including extreme situations without expending time and reducing risk associated to real operation and it can be used for control purposes because a good tradeoff between performance and low complexity is achieved. The procedure followed to obtain the models can be useful for other facilities with similar features. Future work will concentrate on using the developed models for control design purposes and implementing a hierarchical

control strategy to optimize different objectives such as maximizing daily production of distillate, maximize energy efficiency or minimize operating costs.

Acknowledgements

This work has been funded by the National Plan Project DPI2014-56364-C2-1/2-R of the Spanish Ministry of Economy, Industry and Competitiveness and ERDF funds.

References

Alarcón, D.C., Blanco, J., Malato, S., Maldonado, M.I., Fernández, P., 2005. Design and setup of a hybrid solar seawater desalination system: the Aquasol project. ISES 2005 Solar World Congress. Orlando, FL, USA.

Alarcón D. C., García, L., Blanco, J., 2007. Assessment of an absorption heat pump coupled to a multi-effect distillation unit within AQUASOL project. Desalination 212, 303–310.

Alarcón D. C., García, L., Blanco, J., 2010. Design recommendations for a multi-effect distillation plant connected to a double-effect absorption heat pump: A solar desalination case study. Desalination 262, 11–14.

Ayala, C., Roca, L., Guzmán, J., Normey-Rico, J., Berenguel, M., Yebra, L., 2011. Local model predictive controller in a solar desalination plant collector field, Renew. Energ. 36 (2011), 3001-3012.

de la Calle, A., Roca, L., Bonilla, J., Dormido, S., 2015. Modelado y simulación dinámica de procesos termoquímicos en instalaciones termosolares. Documentos CIEMAT.

de la Calle, A., Bonilla, J., Roca, L., Palenzuela, P., 2015. Dynamic modeling and simulation of a solar-assisted multi-effect distillation plant. Desalination, 357, 65–76. doi:10.1016/j.desal.2014.11.008

Camacho, E.F., Berenguel, M., Rubio, F.R., Martínez, D., 2012. Control of Solar Energy Systems, Springer, London.

Carballo, J. A., Bonilla, J., Roca, L., de la Calle, A., Palenzuela, P., Berenguel, M., 2016. Optimal operating conditions analysis of a Multi-Effect Distillation plant. In Desalination for the Environment: Clean Water and Energy. Rome, Italy.

Cirre, C. M., Berenguel, M., Valenzuela, L., Camacho, E.F., 2007. Feedback linearization control for a distributed solar collector field. Control Eng. Prac., 15(12), 1533-1544.

Fernández-Izquierdo, F., García-Rodríguez, L., Alarcón- Padilla, D.C., Palenzuela, P., Martín-Mateos, I., 2012. Experimental analysis of a multi-effect distillation unit operated out of nominal conditions. Desalination 284, 233–237.

Gil, J.D., Ruiz-Aguirre, A., Roca, L., Zaragoza, G., Berenguel, M., 2015. Solar membrane distillation: A control perspective. 23th Mediterranean Conf. on Control and Automation, MED-2015, Málaga, Spain.

Gil, J.D., Ruiz-Aguirre, A., Roca, L., Zaragoza, G., Berenguel, M., 2015a. Control de plantas de destilación por membranas con apoyo de energía solar – parte 1: esquemas. Actas de las XXXVI Jornadas de Automática. Bilbao, Spain.

Gil, J.D., Ruiz-Aguirre, A., Roca, L., Zaragoza, G., Berenguel, M., Guzmán, J.L., 2015b. Control de plantas de destilación por membranas con apoyo de energía solar – parte 2: resultados. Actas de las XXXVI Jornadas de Automática. Bilbao, Spain.

González, R., Roca, L., Rodríguez, F., 2014. Economic optimal control applied to a solar seawater desalination plant. Comput. Chem. Eng., 71, 554–562.

Normey-Rico, J. E. and Camacho, E. F., 2007. Control of Dead-time Processes, Springer, London.

Roca, L., Yebra, L., Berenguel, M., Alarcón D.C., 2006. Control and modeling of seawater desalination using solar technology. 13th Int. Symp. on Concentrated Solar Power and Chemical Energy Technologies. Seville, Spain.

Roca, L., Berenguel, M., Yebra, L., Alarcón D.C., 2008. Solar field control for desalination plants. Sol. Energ. 82, 772–786.

Roca, L., Guzmán, J., Normey-Rico, J., Berenguel M., Yebra J., 2009. Robust constrained predictive feedback linearization controller in a solar desalination plant collector field. Control Eng. Prac. 17, 1076–1088.

Roca, L., Sánchez, J., Rodríguez, F., Bonilla, J., de la Calle, A., Berenguel, M., 2016. Predictive control applied to a solar desalination plant connected to a greenhouse with daily variation of irrigation water demand. Energies, 9(3), 194. doi:10.3390/en9030194.

Romera Cabrerizo, J.A., M. Santos., 2017. ParaTrough: Modelica- based Simulation Library for Solar Thermal Plants. RIAI - Revista Iberoamericana de Automática e Informática Industrial, ISSN: 1697-7912, 14(4):412- 423.

Torrico, B.C., Roca, L., Normey-Rico, J., Guzmán, J., Yebra, L., 2009. Predictive temperature control of solar collectors in a desalination plant. Proc. European Control Conf. 2009, 23–26, Budapest, Hungary.

Torrico, B.C., Roca, L., Normey-Rico, J., Guzmán, J., Yebra, L., 2010. Robust nonlinear predictive control applied to a solar collector field in a solar desalination plant. IEEE Trans. Control Syst. Technol., 18(6), 1430-1439.